Probabilistic estimation of merchant ship source levels in an uncertain shallow-water environment

D. Tollefsen, W. S. Hodgkiss, S. E. Dosso, J. Bonnel, and D. P. Knobles

Submitted : January 3, 2021
Revised : May 28, 2021
Running title : Probabilistic estimation of merchant ship source

D. Tollefsen is with the Norwegian Defence Research Establishment (FFI), Sensor and Surveillance Systems Division, NO-3191 Horten, Norway (e-mail: dag.tollefsen@ffi.no). W. S. Hodgkiss is with the Scripps Institution of Oceanography, University of California San Diego, 9500 Gilman Drive, La Jolla, California 92093-0238, USA (e-mail: wshodgkiss@ucsd.edu). S. E. Dosso is with the School of Earth and Ocean Sciences, University of Victoria, Victoria, British Columbia, Canada V8W 3P6 (e-mail: sdosso@uvic.ca). J. Bonnel is with the Applied Ocean Physics and Engineering Department, Woods Hole Oceanographic Institution, Woods Hole, Massachusetts 02543, USA (e-mail: jbonnel@whoi.edu). D. P. Knobles is with Knobles Scientific and Analysis, Austin, Texas 78755, USA (e-mail: dpknobles@kphysics.org)

DOI til publisert versjon/DOI to published version: 10.1109/JOE.2021.3113506

***Abstract*—** The estimation of ship source levels (SSL) in shallow-water environments can be complicated by sound interaction with the seabed. Uncertainty in seabed properties influence SSL estimates, and it is of interest to mitigate and quantify such effects. This paper proposes a probabilistic approach to ship radiated noise recorded on a vertical line array (VLA) of hydrophones to infer SSL and properties of a mud-sand shallow water seabed on the New England Shelf. The approach, trans-dimensional Bayesian marginalization, samples probabilistically over complex spectral source strengths, source depths/ranges, and number of seabed layers and geoacoustic parameters of each layer. The Bayesian information criterion is applied to determine the appropriate number of (point) sources used to describe a ship. Radiated noise due to two merchant ships passing the VLA at beam aspect at 3.2−3.4 km range is considered. The SSL estimates agree well with reference spectra from shallow-water studies on large ensembles of merchant ships. The average SSL uncertainty (in terms of one-half the inter-quartile range interval) is 3.2 dB/Hz for low-frequency narrowband (20−120 Hz) and 1.8 dB/Hz for broadband noise (190−590 Hz). Seabed layering and geoacoustic parameter estimates agree reasonably well with mud-over-sand seabed models from other inversions in the area.

Index Terms— Ship radiated noise; source level estimation; Bayesian inversion

DOI til publisert versjon/DOI to published version: 10.1109/JOE.2021.3113506

I. INTRODUCTION

Merchant ships are a major contributor to ocean noise in coastal marine environments, especially near shipping lanes leading to and from commercial ports, and it is of interest to obtain information on ship source levels (SSL) from measurements in such settings [1]−[8]. Accurate estimates of SSL are important in predicting and monitoring of shipping noise in marine environments, to address increasing concern about potential effects on marine life [9]. Measurements of SSL typically require a deep-water site and controlled test geometries to minimize environmental effects. For example, the ANSI/ASA standard [10] specifies a minimum distance of the "greater of 100 m or overall ship length" and a minimum water depth of the "greater of 75 m or overall ship length" for survey grade measurements. This can be difficult to achieve with large commercial ships (lengths typically 100−350 m) in coastal environments (water depths typically less than 200 m). Numerical acoustic propagation models can be used to mitigate seabed and multipath effects [2],[3],[5],[8]. This typically assumes a fixed seabed model based on best-available geophysical information for the area of measurement [5],[8], and/or minimizing acoustic data-model differences for an optimal seabed model [2],[3]; however, this does not account for uncertainty in seabed models/parameters in SSL estimates. A further source of uncertainty in SSL estimation is the ship position in range/depth. Accurate ship-to-receiver range can be obtained from ship Automatic Identification System (AIS) data. Source depth models in use include the Gray-Greeley point source model representing propeller noise [11], and a Gaussian-distributed source depth model [5]. These models do not distinguish between different noise-generating mechanisms that can originate from different regions of a ship [12].

Statistical inference on source properties (range/depth and spectral levels of multiple sources) in an uncertain environment was addressed in related work by Dosso and Wilmut on Bayesian source localization [13]. Knobles [14] applied a maximum-entropy inference method for joint SSL and seabed parameter estimation with application to shallow-water data due to a small research vessel. Tollefsen and Dosso [15] developed a Bayesian marginalization approach for SSL estimation that introduced multiple point sources (at uncertain ranges/depths) to represent different noise-generating mechanisms

Dette er en postprint-versjon/This is a postprint version.
DOI til publisert versjon/DOI to published version: 10.1109/JOE.2021.3113506

of a large ship while also treating seabed parameters and layering as uncertain. In the present work, we are primarily interested in SSL estimation of low-frequency narrowband noise (20−120 Hz) of large merchant ships. The approach of [15] is applied with extensions that include: (1) data received on a vertical line array (VLA) in a sloping bottom environment; (2) use of the Bayesian information criterion (BIC) to determine the optimal number of sources; (3) two different assumptions on the character of ship-noise spectral content.

The remainder of this paper is organized as follows. Section II provides a brief overview of the Bayesian marginalization approach applied in this work. Section III describes the acoustic data from the Seabed Characterization Experiment (SBCEX) on the New England Mud Patch, and the seabed and source models used. Section IV presents results in terms of parameter and uncertainty estimates of SSL and seabed geoacoustic profiles. Section V summarizes this paper.

II. THEORY

The Bayesian marginalization approach to SSL estimation is briefly outlined in this section. Trans-dimensional (trans-D) inversion is used to address seabed properties, with implicit sampling over maximum-likelihood (ML) estimates for complex source strengths and error variances (Sec. II-A). Source locations are estimated using Metropolis-Hastings (MH) sampling, with the number of (point) sources inferred using a statistical criterion (Sec. II-B). SSL and uncertainties are estimated from marginal densities for source amplitude (Sec. II-C).

A. Trans-D Bayesian inversion

Trans-dimensional Bayesian inference is used to address unknown seabed layering [16], [17]. In this formulation, Bayes' theorem for a hierarchical model can be written to define the posterior probability density (PPD)

Dette er en postprint-versjon/This is a postprint version.
DOI til publisert versjon/DOI to published version: 10.1109/JOE.2021.3113506

$$P(k,\mathbf{m}_k \mid \mathbf{d}) = \frac{P(k)P(\mathbf{m}_k \mid k)P(\mathbf{d} \mid k,\mathbf{m}_k)}{\sum_{k'\in\mathcal{K}}\int_{\mathcal{M}_{k'}} P(k')P(\mathbf{m}'_{k'} \mid k')P(\mathbf{d} \mid k',\mathbf{m}'_{k'})d\mathbf{m}'_{k'}}, \quad (1)$$

where $\mathcal{M}_k$ represents a M_k–dimensional parameter space, indexed by k, specifying choices of model parameterization with the corresponding sets of M_k free parameters denoted $\mathbf{m}_k$, and $\mathbf{d}$ represents observed data. In (1), $P(k)P(\mathbf{m}_k|k)$ is the prior probability of the state (k, $\mathbf{m}_k$), and $P(\mathbf{d}|k, \mathbf{m}_k)$ is the conditional probability of $\mathbf{d}$ given (k, $\mathbf{m}_k$), which for observed (fixed) data is interpreted as the likelihood of (k, $\mathbf{m}_k$), denoted $L(k, \mathbf{m}_k)$. The PPD is here efficiently sampled using a reversible-jump Markov-chain Monte Carlo (rjMCMC) algorithm with principal-component re-parameterization and parallel tempering [17].

The data considered here consist of complex acoustic pressure fields measured at an N-sensor array and F frequencies at S sub-segments (snapshots) of the acoustic time series, i.e., $\mathbf{d} = \{\mathbf{d}_{fs}, f=1,F; s=1,S\}$. Assuming circularly-symmetric complex Gaussian errors, uncorrelated in space and frequency, with unknown variances v_f which depend on frequency but are considered constant over snapshots and over hydrophones, the likelihood function can be written

$$L(\mathbf{m}) = \prod_{f=1}^{F}\prod_{s=1}^{S}\frac{1}{(\pi v_f)^N}\exp\left[-\left|\mathbf{d}_{fs} - \mathbf{A}e^{i\boldsymbol{\theta}}\mathbf{d}_f(\mathbf{m})\right|^2/v_f\right], \quad (2)$$

where $\mathbf{d}_f(\mathbf{m})$ represents replica data computed for model parameters $\mathbf{m}$ (the index k is omitted for simplicity), and parameters $\mathbf{A}$ and $\boldsymbol{\theta}$ represent unknown source spectra (amplitudes and phases, respectively). The explicit dependence on source spectral parameters and error variances can be removed by substituting analytic maximum-likelihood estimates. Two approaches, based on different assumptions on the source spectra, are derived below.

The *ML incoherent* (MLI) misfit (e.g., [18],[19]) assumes the source amplitude and phase are unknown for each snapshot and frequency (i.e., $\mathbf{A}=\{A_{fs}\}$ and $\boldsymbol{\theta}=\{\theta_{fs}\}$). The MLI source amplitude and phase are estimated by setting $\partial L/\partial A_{fs} = \partial L/\partial\theta_{fs} = 0$ to be:

$$\hat{A}_{fs} = \frac{\left|\mathbf{d}_f^{\mathrm{H}}(\mathbf{m})\mathbf{d}_{fs}\right|}{\left|\mathbf{d}_f(\mathbf{m})\right|^2}, \qquad \hat{\theta}_{fs} = \left[\frac{\mathbf{d}_f^{\mathrm{H}}(\mathbf{m})\mathbf{d}_{fs}}{\mathbf{d}_{fs}^{\mathrm{H}}\mathbf{d}_f(\mathbf{m})}\right]^{1/2}, \quad (3)$$

Dette er en postprint-versjon/This is a postprint version.
DOI til publisert versjon/DOI to published version: 10.1109/JOE.2021.3113506

respectively (see, e.g., [13] for the ML-expression for noise variances.) Substituting the ML estimates for source amplitude and phase and noise variance back into (2) leads to the misfit (negative log-likelihood) function

$$E_{MLI}(\mathbf{m}) = N\sum_{f=1}^{F}\log_e\left\{\mathrm{Tr}\left[\sum_{s=1}^{S}\mathbf{d}_{fs}\mathbf{d}_{fs}^{\mathrm{H}}\right]-\frac{\sum_{s=1}^{S}\left|\mathbf{d}_{fs}^{\mathrm{H}}\mathbf{d}_f(\mathbf{m})\right|^2}{\left|\mathbf{d}_f(\mathbf{m})\right|^2}\right\}. \tag{4}$$

Here, Tr{•} and $^{\mathrm{H}}$ represent the matrix trace and conjugate transpose, respectively.

Alternatively, the *ML amplitude-snapshot* (MLAS) misfit [19] assumes the snapshot-to-snapshot relative amplitude at each frequency is known (the assumption here is that the source amplitude is constant over S snapshots) and phase unknown (i.e., $\mathbf{A}=\{A_f\}$ and $\boldsymbol{\theta}=\{\theta_{fs}\}$). The MLAS source amplitude and phase estimates are

$$\hat{A}_f = \frac{\sum_{s=1}^{S}\left|\mathbf{d}_{fs}^{\mathrm{H}}\mathbf{d}_f(\mathbf{m})\right|}{S\left|\mathbf{d}_f(\mathbf{m})\right|^2}, \qquad \hat{\theta}_{fs} = \left[\frac{\mathbf{d}_f^{\mathrm{H}}(\mathbf{m})\mathbf{d}_{fs}}{\mathbf{d}_{fs}^{\mathrm{H}}\mathbf{d}_f(\mathbf{m})}\right]^{1/2}, \tag{5}$$

respectively, leading to the MLAS misfit function

$$E_{MLAS}(\mathbf{m}) = N\sum_{f=1}^{F}\log_e\left\{\mathrm{Tr}\left[\sum_{s=1}^{S}\mathbf{d}_{fs}\mathbf{d}_{fs}^{\mathrm{H}}\right]-\frac{\left(\sum_{s=1}^{S}\left|\mathbf{d}_{fs}^{\mathrm{H}}\mathbf{d}_f(\mathbf{m})\right|\right)^2}{S\left|\mathbf{d}_f(\mathbf{m})\right|^2}\right\}. \tag{6}$$

Note that in the MLI misfit (4), the measured complex acoustic field over the array for each snapshot and frequency is correlated with the replica field corresponding to that frequency. Hence, the spatial variation of the complex field (amplitude and phase) over the array aperture provides coherent information content. In (4), the magnitude-squared correlations are summed incoherently over snapshots before normalization (by the squared magnitude of the replica field over the array). In the MLAS misfit (6), the correlations are summed incoherently over snapshots; the sum is then squared before normalization. A notable difference is in the ML amplitude estimates: with MLAS, (5), the estimate (for each **m**) is *averaged* over data snapshots; with MLI, (3) provides an amplitude estimate for each snapshot. Explicitly sampling the misfit function [(4) or (6)] over model parameters **m** implicitly samples over the corresponding ML estimates for source spectrum (amplitude and phase) and variances (i.e., for each **m**, amplitude and phase estimates are obtained directly by evaluating equations (3) and (5), respectively).

Dette er en postprint-versjon/This is a postprint version.
DOI til publisert versjon/DOI to published version: 10.1109/JOE.2021.3113506

B. Multiple sources

Multiple point sources are taken to represent different noise generating mechanisms on a ship. Each point source is assigned to represent a specific (unique) set of frequencies, corresponding to a particular noise mechanism, and the misfit function is summed over sources. Metropolis-Hastings sampling is applied to sample the position (depth/range) of each point source (within uniform prior bounds). For the ship dimensions (200−300 m in length and 11−14 m in depth), frequencies (20−590 Hz) and source-receiver ranges (3.2−3.4 km) considered here, the point source assumption is justified assuming sources are distributed along the depth and/or a fraction of the length of the ship.

To determine the most appropriate number of point sources to include in the model for given data, the BIC can be applied [13],

$$\mathrm{BIC} = 2E(\hat{\mathbf{m}}) + H \log_e K\,, \tag{7}$$

where $\hat{\mathbf{m}}$ is the minimum-misfit model, with H the number of model parameters, and K=2FNS the number of data (the factor of 2 accounts for complex measurements). For the MLI misfit, H=N_E+2FS+F+2P; for the MLAS misfit, H=N_E+F(S+1)+F+2P, with N_E the number of environment model parameters (see Sec. III-B). The third term, F, accounts for variances, and the fourth term, 2P, accounts for range and depth for P point sources. Independent inversions are run for an increasing number of sources. The number of point sources yielding a minimum for the BIC is taken to be the most appropriate choice supported by the data.

C. Source Levels

Marginalization for a specific parameter (or pair of parameters) involves integrating the PPD over all other parameters to remove their effect from the resulting one-dimensional (or two-dimensional) marginal probability density. The marginal density for source amplitude A_f is given by marginalizing over environment, source positions, source phase, and noise variances

Dette er en postprint-versjon/This is a postprint version.
DOI til publisert versjon/DOI to published version: 10.1109/JOE.2021.3113506

$$P(A_f|\mathbf{d}) = \int \delta\left(A_f - \hat{A}_f(\mathbf{m})\right) P(\mathbf{m}|\mathbf{d}) d\mathbf{m}, \quad (8)$$

where δ is the Dirac delta function. With MLAS, (8) is applied with the source amplitude estimates from (5). With MLI, one can consider the aggregate (sum) of the marginal densities for the *S* snapshots [15]; alternatively, we apply (for each model **m**) the average of the source amplitude estimates (3) over *S* snapshots $\left[\text{i.e., } \hat{A}_f\ (\mathbf{m}) = S^{-1} \sum_{s=1}^{S} \hat{A}_{fs}(\mathbf{m})\right]$ in (8).

The SSL and uncertainties follow from

$$SSL = 20 \log_{10} \chi \quad (9)$$

with χ a statistical moment of the marginal density (i.e., computed from marginal densities in linear units then converted to decibel scale). The SSL estimate and uncertainty in this work are quantified by the median and one-half the inter-quartile range (IQR) interval, respectively.

III. EXPERIMENT, DATA, AND MODEL

Shallow-water acoustic data were collected during the 2017 Seabed Characterization experiment on the New England Mud Patch [20]. The experiment area (Fig. 1) was located between two major shipping lanes leading to/from the Port of New York and New Jersey. A 16-element VLA of length 56 m was deployed by the Scripps Institution of Oceanography at a water depth of 76.2 m within 3−4 km of the southern shipping lane. Radiated noise from two merchant ships is analyzed (separately) in this work, the data was selected such that there were no other merchant ships within ~50 km range of the ship analyzed.

Dette er en postprint-versjon/This is a postprint version.
DOI til publisert versjon/DOI to published version: 10.1109/JOE.2021.3113506

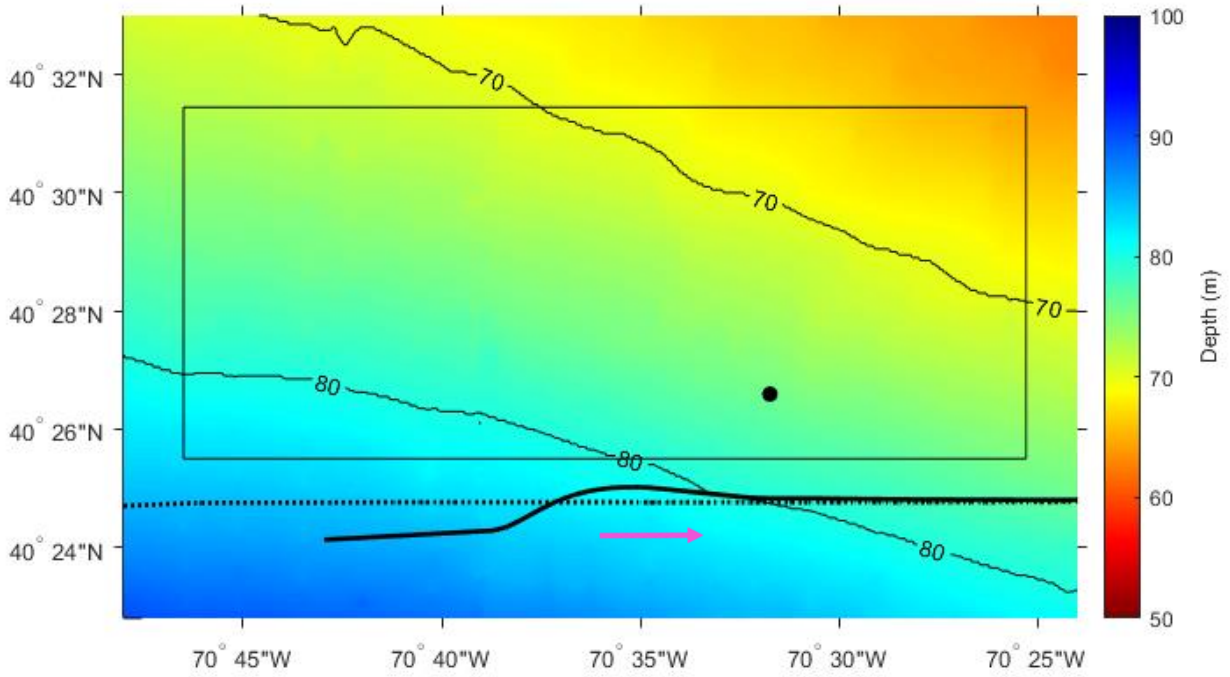

Fig. 1. NOAA bathymetry (color, 10 m isobaths), experiment area (box), location of the VLA (circle), ship AIS tracks for the vehicle carrier *Tombarra* (black dotted) and container ship *Kalamata* (black solid), and ship directions (purple arrow).

A. Acoustic data

The vehicle carrier *Tombarra* (see Table I for ship specifications) passed the VLA at beam aspect with a closest point of approach (CPA) on March 31st at 104300 UTC at a range of 3.41 km south of the array. Fig. 2(a) shows the spectrogram from a single hydrophone recording of the ship passage. Distinct frequency lines within the frequency band 15–120 Hz are related to propeller and machinery generated noise. Analysis of the noise spectrogram identified five prominent narrowband frequencies included in the inversions (labeled NB: 21, 32, 60, 90, and 120 Hz). Knowledge of the ship's parameters (Table I) allowed for these frequencies to be related to tonals associated with machinery noise (labeled F: 21, 32 Hz) and with propeller noise (labeled B: 60, 90, 120 Hz). In addition, 21 frequency components representing broadband noise (BB: 190−590 Hz) were included in the analysis. Data vectors were formed from time-series data, centered around the CPA time, sampled at 25 kHz, using spectral estimation with 1-Hz FFT resolution over S=8 consecutive, non-overlapping snapshots, each of duration 1 s; the ship moved approximately 70 m over the 8 s data segment.

Dette er en postprint-versjon/This is a postprint version.
DOI til publisert versjon/DOI to published version: 10.1109/JOE.2021.3113506

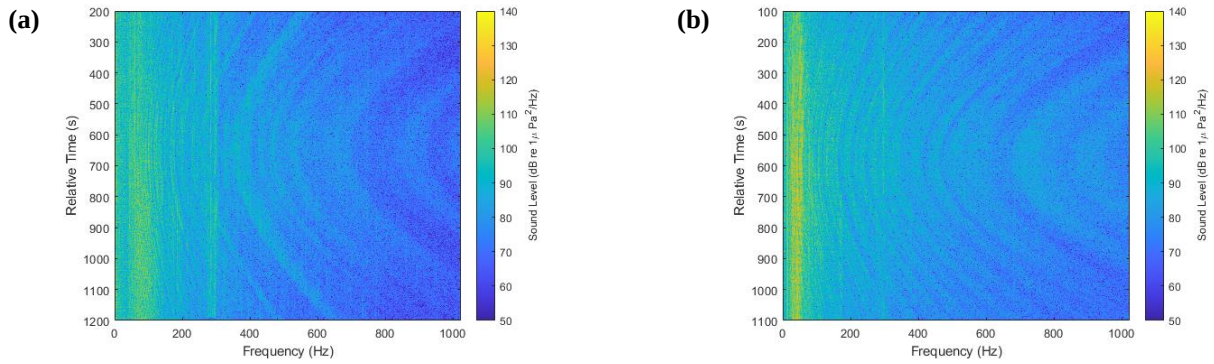

Fig. 2. Spectrograms of received noise due to (a) the vehicle carrier *Tombarra*, (b) the container ship *Kalamata*.

The container ship *MSC Kalamata* approached from the west and passed the VLA with a CPA on March 24th at 183030 UTC at a range of 3.28 km south of the array. Fig. 2(b) shows the spectrogram from a single hydrophone recording of the container ship passage. Analysis of the noise spectrogram and knowledge of the ship's parameters (Table I) identified five narrowband frequencies included in the inversions (NB: 21, 28, 41, 76, and 96 Hz). The multiplicative factor between number of engine cylinders (10) and number of propeller blades (5) prevented a further delineation into machinery- and propeller-related tonals for this ship. In addition, 21 broadband components (BB: 190−590 Hz) were included in the analysis. The data processing was similar to the description above.

TABLE I

SHIP PARAMETERS (*-ASSUMED).

Parameter and units	*Tombarra*	*MSC Kalamata*
IMO Number	9319753	9244946
Gross Tonnage (T)	22,149	74,656
AIS draft (m)	9.3	11.0
Maximum draft (m)	11.0	14.0
Length overall (m)	200.0	303.8
Breadth extreme (m)	32.3	40.0
Maximum capacity (TEU)	-	6242
Year built	2006	2003
Number of cylinders	7	10
Number of propeller blades	5	5
Ship speed (kn)	17.1	19.9
Shaft RPM	90*	70.7*

B. Environment model and prior information

Water depths along the ship-to-array tracks were inferred from a bathymetric model based on SBCEX data collected with a multi-beam bottom profiler [20], and from data downloaded from the NOAA

Dette er en postprint-versjon/This is a postprint version.
DOI til publisert versjon/DOI to published version: 10.1109/JOE.2021.3113506

NCEI data center. Water depths are within 76.2–80.5 m, with an approximately constant slope of 0.075°. Bathymetry was parameterized by a water depth at the CPA position (source), and by a depth difference to the array position (receiver), assuming a constant slope in between.

Wide uniform prior bounds for water depth at the CPA position of 76.5−84.5 m (nominal 80.5 m for the *Kalamata*), and for depth difference to the array of −4.8 to −3.8 m (nominal −4.3 m) were used (equivalent to a slope of 0.066°−0.084°). To allow for uncertain VLA geometry, the VLA deepest element elevation above the seabed (4−6 m, nominal 5.0 m), and VLA tilt (−3° to +3°, nominal 1.0° estimated from a tilt sensor at the top of the array) were also included as parameters in the inversions. A straight-line array was assumed. To account for a sloping bottom, the RAM parabolic equation propagation model [21], the version that assumes seabed layers parallel to the bathymetry, was used to compute all replica data, $\mathbf{d}_f(\mathbf{m})$, in the inversions.

The model environment consists of a water column (range-dependent depth) with a sound speed profile (SSP) over a layered seabed (range independent layer thickness and properties within layers). The SSP was constructed based on temperature data from 22 sensors along the VLA mooring, data recorded at the time of the acoustic data, and salinity data from a CTD measurement taken within 12 hrs of the acoustic data, and within 1.3 km of the VLA. The temperature profile for March 24th indicated well-mixed water of near-constant temperature (+5.4° C); sound speed increased from 1469.9 m/s at the surface to 1471.3 m/s at the seabed. The temperature profile for March 31st also indicated well-mixed water (at +6.1° C); sound speed increased from 1473.1 m/s at the surface to 1474.1 m/s at the seabed.

The parameters that describe each homogeneous seabed layer are the interface depth (z_k), sound speed (c_k), density (ρ_k) and attenuation coefficient (α_k). Uniform prior bounds were set to 1440−2100 m/s for sound speed, 1.2−2.4 g/cm³ for density, and 0−0.5 dB/λ for attenuation in each seabed layer. Sound speed and density were also constrained by a two-dimensional (2D) joint prior density based on Hamilton's empirical relations [22]. We used k=1−3 as the bounds for the number of seabed layer interfaces to a maximum depth of 30 m; the number of interfaces and the maximum depth are reasonable choices based on results from a previous ship-noise data inversions in this area [23]. In the

Dette er en postprint-versjon/This is a postprint version.
DOI til publisert versjon/DOI to published version: 10.1109/JOE.2021.3113506

BIC, the number of environment parameters is then $N_E = 4k + 3$ (array and water depth parameters for simplicity omitted).

C. Source model

Ship range was inferred from AIS data obtained from the United States Coast Guard Navigation Center Nationwide AIS database. Prior uniform bounds on range were set to $r_{AIS} \pm 150$ m, with r_{AIS} the ship AIS position to array range. Prior uniform bounds on source depth were set to 1−14 m. Inversions were run with 1, 2, and 3 point sources for the *Tombarra*, and 1 and 2 sources for the *Kalamata*. When 2 sources were used, one source (NB) was taken to represent all narrowband frequencies and one source (BB) was taken to represent broadband noise. When 3 sources were used, one source represented each set of frequencies for propeller noise (B), machinery noise (F), and broadband noise (BB), respectively.

D. Sampling and convergence

Trans-D sampling was run with ten rjMCMC chains in parallel tempering. The results presented here are for 20,000 samples from the unit-temperature chain, collected after an initial burn-in over 10,000 samples. A chain thinning factor of 2 was applied (i.e., every second sample saved). Convergence was determined by comparing marginal densities from the first and second halves of the total sample, checking that the marginal densities did not differ significantly.

IV. RESULTS

A. Number of sources, source depth, and source range

Inversions of radiated noise due to the *Tombarra* are discussed first. Fig. 3 (upper panels) shows the minimum misfits with E_{MLI} and E_{MLAS} from independent inversions with 1, 2, and 3 sources. The lowest misfit is obtained with three sources, both with E_{MLI} and with E_{MLAS}. Fig. 3 (lower panels) shows the

Dette er en postprint-versjon/This is a postprint version.
DOI til publisert versjon/DOI to published version: 10.1109/JOE.2021.3113506

BIC for the minimum-misfit models. For all numbers of sources, the BIC with MLAS is lower than with MLI. Both with MLI and with MLAS, the minimum BIC is with two sources. The lowest overall BIC is with

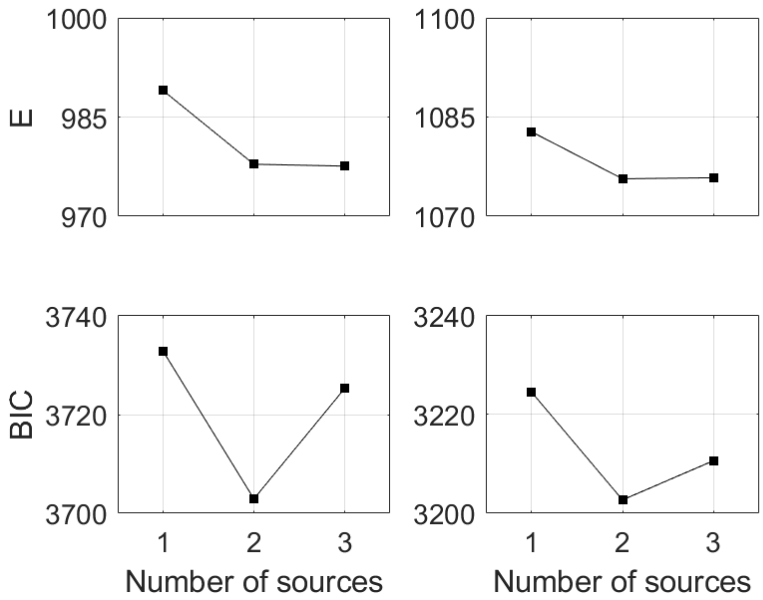

Fig. 3. Results from Bayesian inversion of radiated noise due to the *Tombarra*: minimum misfit (upper panels) and the BIC (lower panels) for 1−3 point sources representing the ship. Results are with the MLI misfit (left panels) and with the MLAS misfit (right panels).

MLAS and with two sources. This suggests the appropriate misfit, MLAS, and number of sources, two, for these data (used in the following, unless otherwise noted).

Fig. 4 shows the 2D marginal probability densities for source range/depth (left panels), and marginal probability density for source depth (right panels) for the inversions with one source [Fig. 4(a)] and with two sources [Fig. 4(b)]; the one-source model result is plotted for comparison. With one source, Fig. 4(a), the median with one-half IQR uncertainty is 3.40±0.001 km in range and 6.3±0.7 m in depth. The range uncertainty is negligible and the estimate is within 0.01 km (less than the ship's breadth) of the range estimated from AIS data. The uncertainty in depth is also relatively narrow. With two sources, for the first source (NB) representing all narrowband frequencies [Fig. 4(b), upper panel] the uncertainty is narrow in range, but extends over most of the prior interval in depth. The medians with one-half IQR

Dette er en postprint-versjon/This is a postprint version.
DOI til publisert versjon/DOI to published version: 10.1109/JOE.2021.3113506

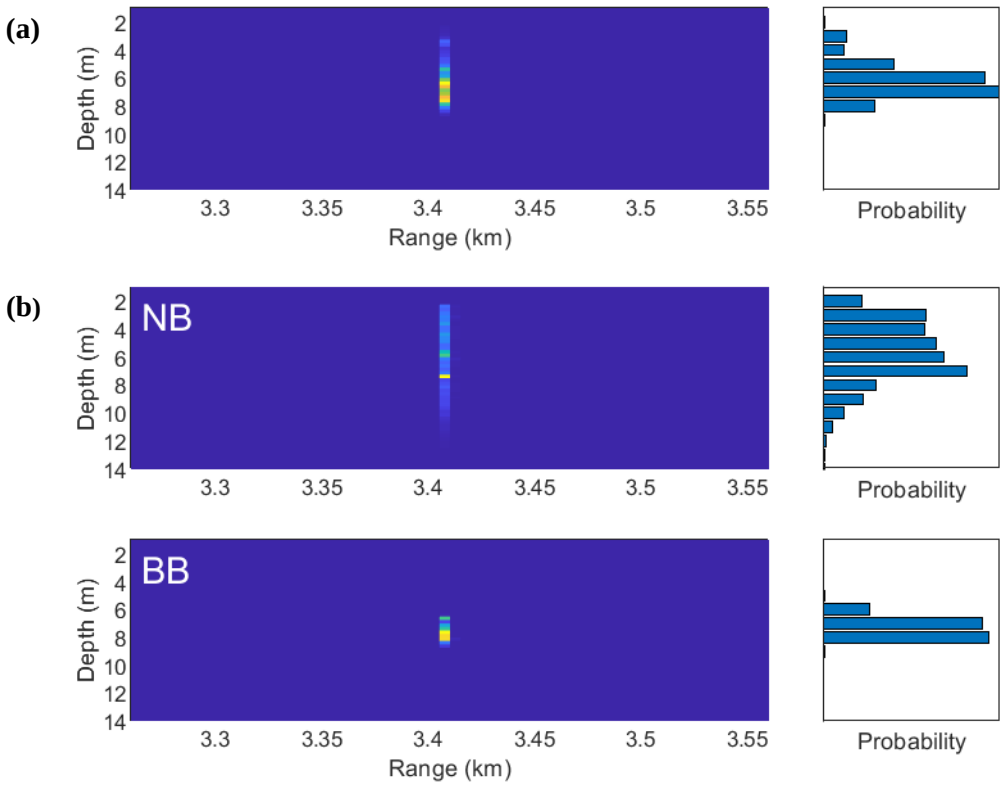

Fig. 4. Results from inversion of radiated noise due to the *Tombarra* at beam aspect: 2D source range/depth marginal probability density (left) and marginal probability density for source depth (right) for inversion with (a) 1 point source, and (b) 2 point sources (see text for an explanation of labels NB and BB).

uncertainties are 3.40±0.001 km and 5.6±1.5 m, respectively. For the second source (BB) representing all broadband frequencies [Fig. 4(b), lower panel], the uncertainty is narrow also in depth, with median with one-half IQR uncertainty 7.4±0.4 m. The increased depth of the second source is consistent with the observation in [4] that "the apparent depth for high-frequency wideband noise is deeper (than propeller-generated noise), possibly because this is the region where tip cavities streaming off the blades collapse". The median depth of the first source is consistent with the Gray-Greeley model [11] for propeller noise (with ship draft 9.3 m, a source depth of 5.3 m). Results with three sources, not shown, were qualitatively similar to those with two sources: for source range, narrow distributions centred near the nominal range, for source depth a narrow distribution for the source representing broadband frequencies with wider distributions centered at shallower depths for the two sources representing narrowband frequencies.

Dette er en postprint-versjon/This is a postprint version.
DOI til publisert versjon/DOI to published version: 10.1109/JOE.2021.3113506

Inversions of radiated noise due to the *Kalamata* were run with 1 and 2 sources; a three-source model is not possible for this ship (see Sec. III-A). The 2D marginal probability densities for source range/depth were qualitatively similar to those presented for the *Tombarra*. For example, with two sources, the median with one-half IQR uncertainties for depth were 7.3±2.6 m for the first (NB) source and 8.0±0.5 m for the second (BB) source.

B. Seabed geoacoustic profiles

Fig. 5(a) shows the geoacoustic marginal probability profiles from inversions of radiated ship noise due to the *Tombarra.* The profiles indicate a low-speed/low-density iso-speed upper layer, an interface/transition at 7−10 m depth (most of the probability is concentrated around 7−8 m, a tail extends to 10 m), and a higher-speed/higher-density layer below. The profiles are overall consistent with the layered mud-over-sand sediment model from other inversions in the Mud Patch [20]. Table II (left column) provides the mean and mean deviation values for the seabed parameters (this uncertainty measure is often adopted for seabed parameters), at depths of 0 m (at the top of the mud layer) and at 12 m (beneath the mud layer). At 0 m, the estimates are 1473.4±0.7 m/s and 1.53±0.05 g/cm^3, respectively, for sound speed and density. At 12 m depth, the estimates are 1958±62 m/s and 2.16±0.06 g/cm^3, respectively, for sound speed and density. There is an indication in the sound speed profile of a possible intermediate layer at ~7 m depth, beneath the upper mud layer. At 7 m depth, mean with mean-deviation estimates are 1567±99 m/s and 1.69±0.18 g/cm^3, respectively, for sound speed and density. The layering is reasonably consistent with a model developed from chirp seismic reflection survey data [20]: at the VLA site, the model yields an upper (mud) layer of thickness ~11 m (here estimated using two-way travel time from the model and a layer sound speed of 1473.4 m/s) followed by a <1 m thick layer (sand) over deeper (unidentified) layers.

Dette er en postprint-versjon/This is a postprint version.
DOI til publisert versjon/DOI to published version: 10.1109/JOE.2021.3113506

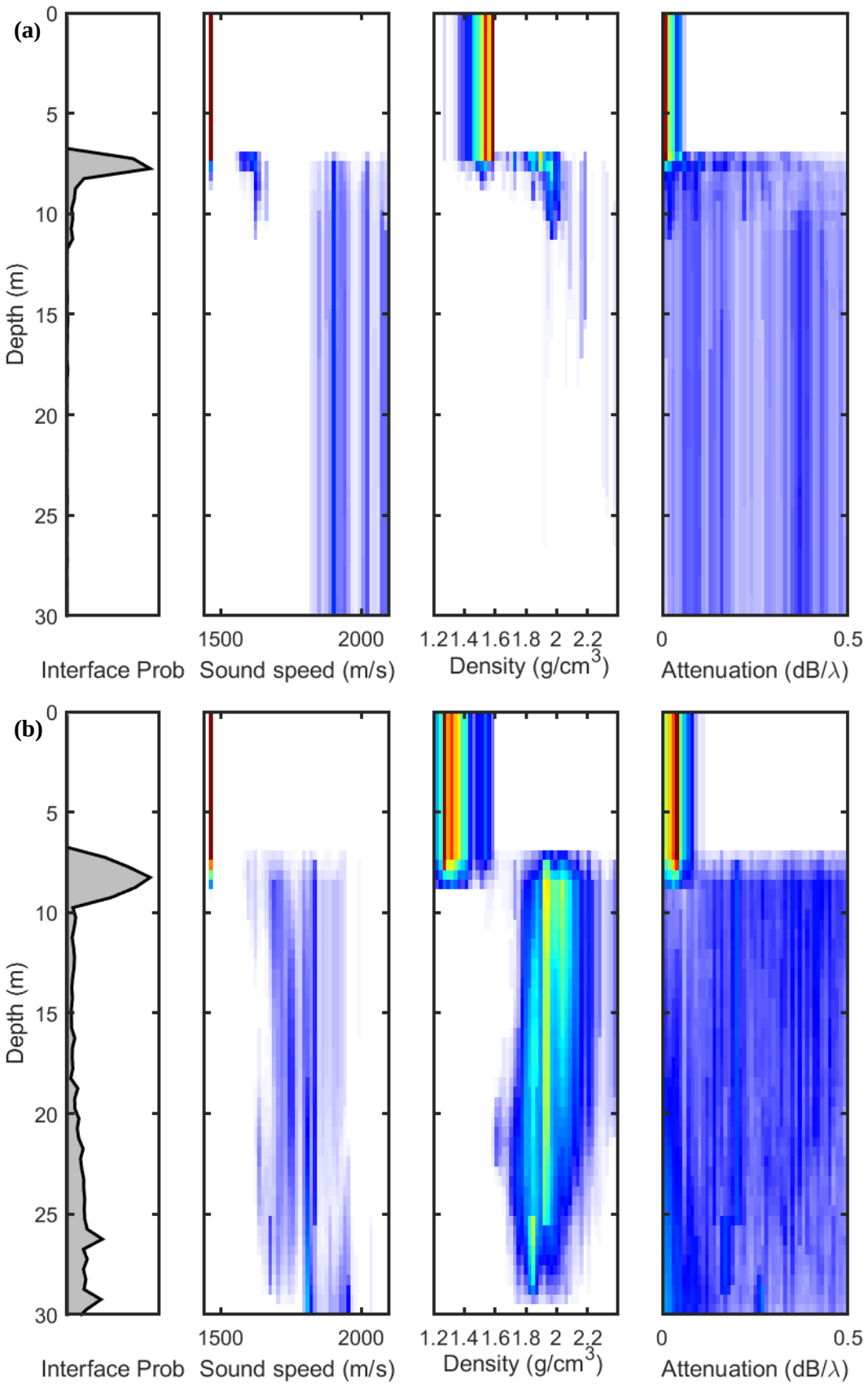

Fig. 5. Geoacoustic marginal probability profiles from inversion of radiated noise due to (a) the *Tombarra*, and (b) the *Kalamata*. (Warmer colors indicate regions of higher probability and white is zero).

Dette er en postprint-versjon/This is a postprint version.
DOI til publisert versjon/DOI to published version: 10.1109/JOE.2021.3113506

Fig. 5(b) shows the geoacoustic marginal probability profiles from inversions of radiated ship noise due to the *Kalamata*. The profiles are qualitatively similar to those obtained from inversions of data from the *Tombarra* over approximately the same source-receiver track: both inversions indicate a low-velocity/low-density upper seabed layer over a higher-velocity/higher-density layer with a transition at 7−10 m depth, and there is considerable overlap in the probability distributions of the sound speed in the lower layer. Table II (right column) provides the mean and mean deviation values for the seabed parameters. For the top of the mud layer, the sound speed estimate is 1473.1±0.5 m/s and the density estimate is 1.36±0.06 g/cm^3. Below the mud layer (at 12 m depth), the estimates are 1785±58 m/s for sound speed and 1.99±0.10 g/cm^3 for density. The estimates for the mud layer are reasonably consistent with results from other SBCEX inversions in this part of the experiment area, e.g., Bonnel et *al*. [22]: 1471 m/s and 1.56 g/cm^3 from inversion of modal dispersion data at a nearby location (see [20] for an overview of further results).

TABLE II

SEABED PARAMETERS AND UNITS, AND INVERSION PARAMETERS MEAN AND MEAN-DEVIATION UNCERTAINTY ESTIMATES.

Parameters and units	Depth (m)	*Tombarra*	*MSC Kalamata*
Sound speed (m/s)	0	1473.4±0.7	1473.1±0.5
	12	1958±62	1785±58
Density (g/cm^3)	0	1.53±0.05	1.36±0.06
	12	2.16±0.10	1.99±0.10
Attenuation (dB/λ)	0	0.02±0.01	0.04±0.02
	12	0.28±0.12	0.27±0.12

C. Source levels and uncertainties

Fig. 6 shows marginal probability densities for SSL for the *Tombarra*, for two narrowband and one broadband frequency component, in dB re μPa^2 m^2/Hz (dB/Hz). For display purposes, these probability densities were computed in dB units, using a bin width of 3 dB. The densities are unimodal. Table III (left columns) shows the median SSL estimates and uncertainty (in terms of one-half the IQR interval) for the narrowband frequencies.

Dette er en postprint-versjon/This is a postprint version.
DOI til publisert versjon/DOI to published version: 10.1109/JOE.2021.3113506

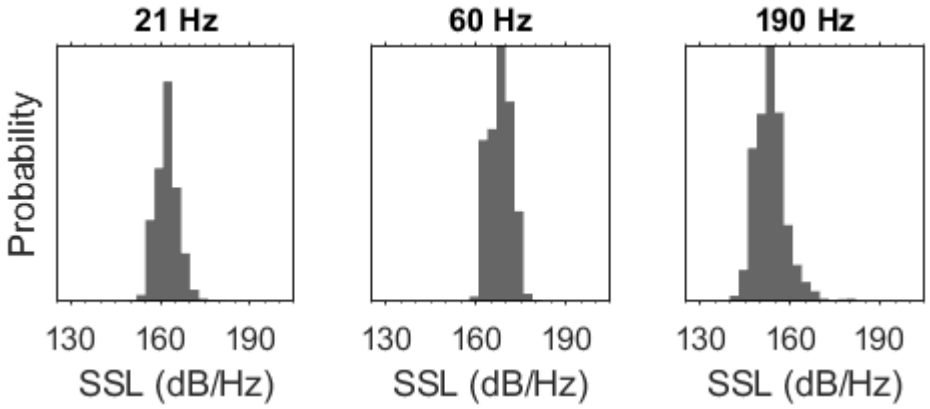

Fig. 6. Marginal probability densities for SSL at three frequencies, from inversion of radiated noise due to the *Tombarra.*

TABLE III

FREQUENCY AND LABEL (B−PROPELLER-RELATED, F−MACHINERY-RELATED, THE NUMBER INDICATES INDEX IN A HARMONIC SERIES), MEDIAN SSL ESTIMATE, AND SSL UNCERTAINTY IN TERMS OF ONE-HALF THE INTER-QUARTILE RANGE (IQR) INTERVAL, FROM INVERSIONS OF NARROWBAND RADIATED NOISE DUE THE VEHICLE CARRIER *TOMBARRA* (LEFT THREE COLUMNS) AND THE CONTAINER SHIP *KALAMATA* (RIGHT THREE COLUMNS), AT BEAM ASPECT.

Tombarra			*MSC Kalamata*		
Frequency (Hz)	SSL (dB/Hz)	SSL uncertainty (dB/Hz)	Frequency (Hz)	SSL (dB/Hz)	SSL uncertainty (dB/Hz)
21 (F2)	161.6	4.0	21	182.3	3.4
32 (F3)	159.2	3.3	28	175.7	3.4
60 (B8)	167.4	3.2	41	175.1	3.2
90 (B12)	159.8	2.9	76	166.3	2.9
120 (B16)	164.2	2.7	96	158.8	2.4

Fig. 7(a) shows the SSL estimates and uncertainties. The error bars indicate the upper and lower quartiles and the symbol is the median. The solid curve is the Wales-Heitmeyer (WH) reference spectrum [5] based on the mean of 54 merchant ship measurements. The dashed curve is the mean of a large ensemble of measurements on vehicle carriers in shallow water (Fig. 6 of [3], adjusted for processing bandwidth). The highest estimated SSL is 167.4 dB/Hz at 60 Hz (B8). The SSL estimates at the two lowest frequencies (F2 and F3) are lower: 161.6 dB/Hz at 21 Hz and 159.2 dB/Hz at 32 Hz. At 190−290 Hz, the SSL estimates are close to the WH curve; above ~300 Hz, the SSL estimates deviate to higher

Dette er en postprint-versjon/This is a postprint version.
DOI til publisert versjon/DOI to published version: 10.1109/JOE.2021.3113506

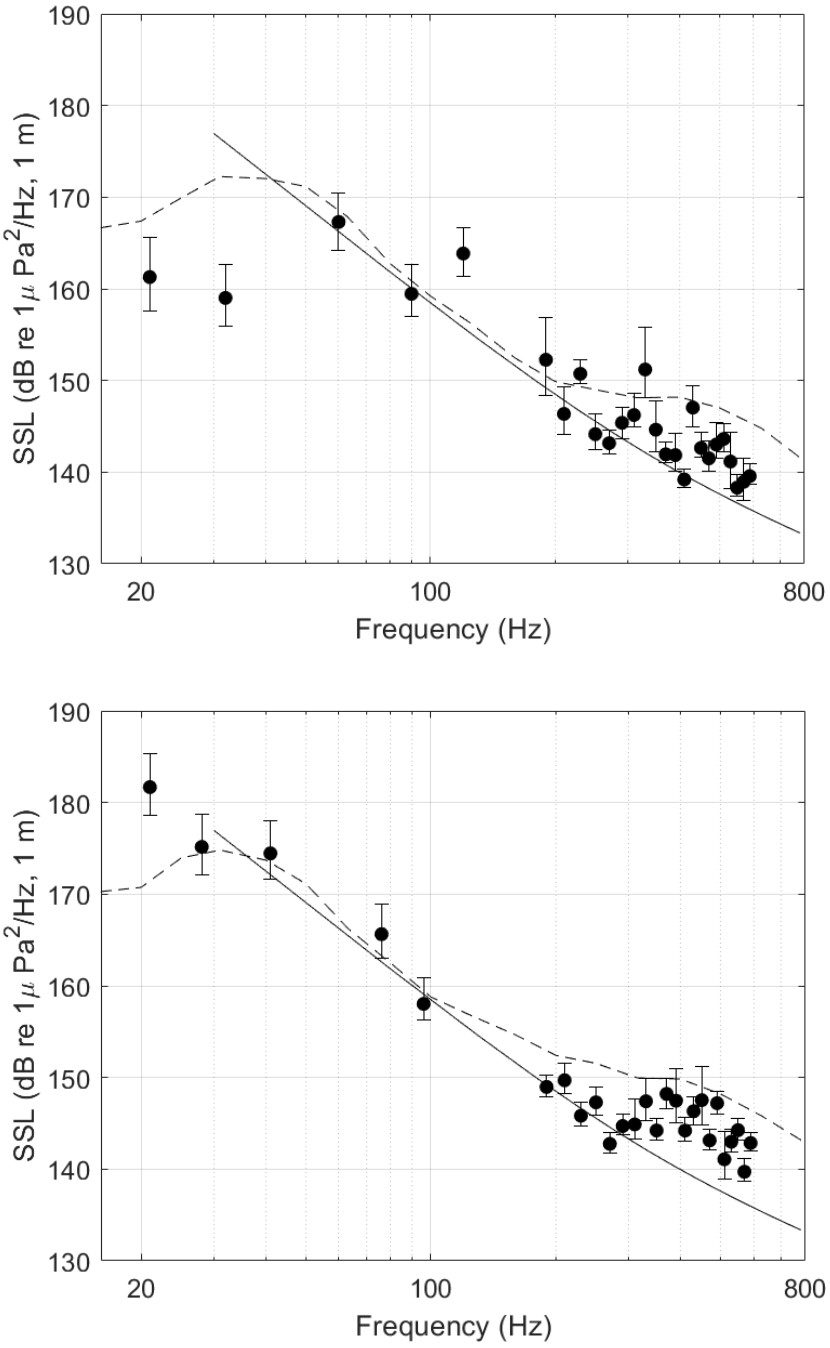

Fig. 7. Median SSL estimates (symbols) with inter-quartile range uncertainty intervals (bars), from inversion of radiated noise due to the vehicle carrier *Tombarra* (upper panel) and the container ship *MSC Kalamata* (lower panel). The solid curve is the Wales-Heitmeyer spectrum [5] based on the mean of 54 measurements on merchant ships. The dashed curves are mean spectra based on measurements on vehicle carriers (upper panel) and container ships (lower panel) in shallow water [3].

levels than the WH curve in a manner analogous to the Ref. [3] curve. The dB-average SSL uncertainties are 3.2 dB/Hz for the narrowband and 2.0 dB/Hz for the broadband frequencies.

Dette er en postprint-versjon/This is a postprint version.
DOI til publisert versjon/DOI to published version: 10.1109/JOE.2021.3113506

Fig. 7(b) shows the SSL estimates and uncertainties for the *Kalamata*. The dashed curve is here the mean of a large ensemble of measurements on container ships (from [3]). The SSL estimates for the narrowband frequencies are in overall good agreement with the WH curve. At 21 Hz, the SSL estimate is approximately 12 dB above the Ref. [3] curve. Above ~300 Hz, the SSL estimates deviate to higher SSLs than the WH curve, in a manner analogous to the Ref. [3] curve. The dB-average SSL uncertainties are 3.2 dB/Hz for the narrowband and 1.6 dB/Hz for the broadband frequencies.

It can be of interest to compare the SSL estimates obtained with MLAS with those obtained using the MLI misfit. Overall, the SSL estimates with MLI are within 2 dB of estimates with MLAS. Note that the estimates with MLI and with MLAS are from independent inversions, with small differences in estimated seabed geoacoustic profiles and source depths/ranges. The dB-average SSL uncertainties with MLI are 3.9 dB/Hz for narrowband and 3.7 dB/Hz for broadband frequencies. With MLI and averaging over snapshots (see Sec. II-C), the uncertainties are 2.8 dB/Hz for narrowband and 1.5 dB/Hz for broadband frequencies (with MLAS: 3.2 dB/Hz and 1.6 dB/Hz, respectively). Averaging over data snapshots is customary in SSL measurements: for example, the ANSI/ASA standard [10] for precision method narrowband measurements specifies an averaging time of ≤1 s; for survey method measurements the standard specifies an averaging time of ~30 s for the ships and ranges considered here.

V. SUMMARY

This paper proposed a Bayesian marginalization approach to ship spectral source level estimation with uncertain environment and a source model that used multiple point sources (of uncertain depths/ranges) to describe a ship. The algorithm applied trans-D rjMCMC sampling of a seabed of *a priori* unknown layering and properties, Metropolis-Hastings sampling over source depths/ranges and over water depth and array parameters, implicit sampling over the maximum-likelihood estimates for complex source strengths and error variances, and determined the number of sources using the BIC. Marginal densities for source strength were derived, with SSL estimates and uncertainties derived from

Dette er en postprint-versjon/This is a postprint version.
DOI til publisert versjon/DOI to published version: 10.1109/JOE.2021.3113506

the densities. While it is a seemingly attractive concept also to apply trans-D sampling over the number of sources, there are theoretical and practical issues related to the large number of parameters per source (range, depth and amplitudes/phases at all frequencies) that makes this infeasible, although it has been accomplished within an optimization framework [24].

The approach was applied to radiated noise due to two merchant ships, a vehicle carrier and a container ship, recorded on a VLA in shallow water on the New England Mud Patch. The BIC indicated that two point sources were the most appropriate to describe the *Tombarra*: one source to represent narrowband frequencies and one source to represent broadband radiated noise. The source depth marginal densities differed between these sources; for the source representing broadband noise, a narrow density centered in the lower half of the ship draft; for the source representing narrowband frequencies, a wider density centered near one-half of the ship's draft. Two different assumptions on the relative source amplitude between data snapshots were applied: unknown, or known in a relative sense (amplitude constant over snapshots). The BIC indicated that the second assumption was the most appropriate with these data.

The SSL measurements were conducted in shallow water (depth 76−82 m) at long range (3.2−3.4 km), over a seabed of *a priori* uncertain layering and composition. The seabed properties estimated from radiated ship noise agreed well with a mud-over-sand seabed model for the area. Within uncertainties, the SSL estimates agreed reasonably well with reference spectra reported for large ensembles of measurements on merchant ships. The average SSL uncertainties, in terms of one-half the IQR intervals, were 3.2 dB/Hz for low-frequency narrowband (20−120 Hz) and 1.8 dB/Hz for broadband radiated noise (190−590 Hz).

A more general study could also consider effects of data error correlations on SSL uncertainties; for example, at the lowest frequencies analyzed, uncertainties may be underestimated due to correlations neglected in the present study. Finally, while ship radiated noise is known to vary with aspect angle [4],[7], SSLs were here reported for beam aspect only. The approach developed is applicable to other ship aspects; however, this was considered less practical for the ship tracks of the present data set due to the longer ranges required.

Dette er en postprint-versjon/This is a postprint version.
DOI til publisert versjon/DOI to published version: 10.1109/JOE.2021.3113506

ACKNOWLEDGMENT

Support for this work was provided by the Office of Naval Research, and by FFI. The authors wish to thank the crew of the *R/V Endeavor*. Kai Abrahamsen of DnV-GL Maritime provided insight on ship parameters.

REFERENCES

[1] L. Hatch et al., "Characterizing the Relative Contributions of Large Vessels to Total Ocean Noise Fields: A Case Study Using the Gerry E. Studds Stellwagen Bank National Marine Sanctuary," *Environmental Management*, vol. 42, pp. 735–752, 2008.

[2] Y. Simard, N. Roy, C. Gervaise, and S. Giard, "Analysis and modeling of 255 source levels of merchant ships from an acoustic observatory along St. Lawrence Seaway," *J. Acoust. Soc. Amer.*, vol. 140, pp. 2002–2018, 2016.

[3] A. O. MacGillivray, Z. Li, D. E. Hannay, K. B. Trounce, and O. M. Robinson, "Slowing deep-sea commercial vessels reduces underwater radiated noise," *J. Acoust. Soc. Amer.*, vol. 146, pp. 340–351, 2019.

[4] P. T. Arveson and D. J. Vendittis, "Radiated noise characteristics of a modern cargo ship," *J. Acoust. Soc. Amer.*, vol. 107, pp. 118–129, 2000.

[5] S. C. Wales and R. M. Heitmeyer, "An ensemble source spectra model for merchant-ship generated noise," *J. Acoust. Soc. Amer.*, vol. 111, pp. 1211–1231, 2002.

[6] M. F. McKenna, D. Ross, S. M. Wiggins, and J. A. Hildebrand, "Underwater radiated noise from modern commercial ships," *J. Acoust. Soc. Amer.*, vol. 131, pp. 92–103, 2012.

[7] M. Gassmann, S. M. Wiggins, and J. A. Hildebrand, "Deep-water measurements of container ship radiated noise signatures and directionality," *J. Acoust. Soc. Amer.*, vol. 142, pp. 1563–1574, 2017.

[8] J. S. Rogers, S. C. Wales, and S. L. Means, "Ambient noise forecasting with a large acoustic array in a complex shallow water environment," *J. Acoust. Soc. Amer.*, vol. 142, pp. EL473–EL477, 2017.

[9] C. Erbe, S. A. Marley, R. P. Schoeman, J. N. Smith, L. E. Trigg, C. B. Embling, "The Effects of Ship Noise on Marine Mammals—A Review," *Front. Mar. Sci.*, vol. 6:606, 2019.

[10] ANSI/ASA, S12.64/Part 1, *American National Standard Quantities and Procedures for Description and Measurement of Underwater Sound from Ships Part 1: General Requirement*s (American National Standards Institute and Acoustical Society of America, New York, 2009).

[11] L. M. Gray and D. S. Greeley, "Source level model for propeller blade radiation for the world's merchant fleet," *J. Acoust. Soc. Amer.*, vol. 67, pp. 516–522, 1980.

Dette er en postprint-versjon/This is a postprint version.
DOI til publisert versjon/DOI to published version: 10.1109/JOE.2021.3113506

[12] D. Wittekind, “A simple model for the underwater noise source level of ships,” *J. Ship. Prod. Des*., vol. 30, pp. 1–8, 2014.

[13] S. E. Dosso and M. J. Wilmut, “Bayesian multiple-source localization in an uncertain ocean environment,” *J. Acoust. Soc. Amer*., vol. 129, pp. 3577–3589, 2011.

[14] D. P. Knobles, “Maximum entropy inference on seabed attenuation parameters using ship radiated broadband noise,” *J. Acoust. Soc. Amer*., vol. 138, pp. 3563–3575, 2015.

[15] D. Tollefsen and S. E. Dosso, “Ship source level estimation and uncertainty quantification in shallow water via Bayesian marginalization,” *J. Acoust. Soc. Amer*., vol. 147, pp. EL339–EL344, 2020.

[16] J. Dettmer and S. E. Dosso, “Trans-dimensional matched-field geoacoustic inversion with hierarchical error models and interacting Markov chains,” *J. Acoust. Soc. Amer*., vol. 132, pp. 2239–2250, 2012.

[17] S. E. Dosso, J. Dettmer, G. Steininger and C. W. Holland, “Efficient trans-dimensional Bayesian inversion for geoacoustic profile estimation,” *Inverse Problems*, vol. 30, 114018, 29 pp., 2014.

[18] P. Gerstoft and C. F. Mecklenbräuker, “Ocean acoustic inversion with estimation of *a posteriori* probability distributions,” *J. Acoust. Soc. Amer.*, vol. 104, pp. 808-819, 1998.

[19] S. E. Dosso and M. J. Wilmut, “Maximum-likelihood and other processors for incoherent and coherent matched-field localization,” *J. Acoust. Soc. Amer*., vol. 132, pp. 2273-2285, 2012.

[20] P. S. Wilson, D. P. Knobles, and T. B. Neilsen, “An overview of the seabed characterization experiment,” *IEEE J. Oceanic Eng.*, vol. 45, pp. 1–13, 2020.

[21] M. D. Collins, “A split-step Padé solution for the parabolic equation method,” *J. Acoust. Soc. Amer*., vol. 93, pp. 1736–1742, 1993.

[22] J. Bonnel, S. Dosso, D. Eleftherakis, and R. Chapman, “Trans-dimensional inversion of modal dispersion data on the New England Mud Patch,” *IEEE J. Ocean. Eng.*, vol. 45, pp. 116–130, 2020.

[23] D. Tollefsen, S. E. Dosso, and D. Knobles, “Ship-of-opportunity noise inversions for geoacoustic profiles of a layered mud-sand seabed,” *IEEE J. Ocean. Eng.*, vol. 45, pp. 189–200, 2020.

Dette er en postprint-versjon/This is a postprint version.
DOI til publisert versjon/DOI to published version: 10.1109/JOE.2021.3113506

[24] S. E. Dosso, J. Dettmer, and M. J. Wilmut, “Efficient localization and spectral estimation of an unknown number of ocean acoustic sources using a graphics processing unit,” *J. Acoust. Soc. Amer.*, vol. 138, pp. 2945−2956, 2015.